



Original Research

Reconstruction of rabbit mandibular bone defects using carbonate apatite honeycomb blocks with an interconnected porous structure

Keiko Kudoh¹ · Naoyuki Fukuda¹ · Kazuya Akita¹ · Takaharu Kudoh¹ · Natsumi Takamaru¹ · Naito Kurio¹ · Koichiro Hayashi¹ · Kunio Ishikawa² · Youji Miyamoto²

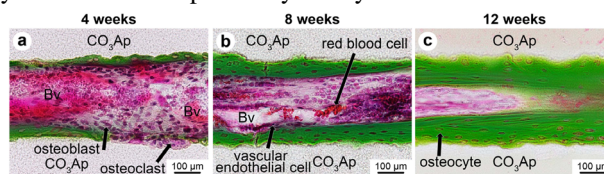
Received: 18 March 2022 / Accepted: 5 December 2022 / Published online: 31 December 2022
© The Author(s) 2022

Abstract

Carbonate apatite (CO₃Ap) granules are useful as a bone substitute because they can be remodeled to new natural bone in a manner that conforms to the bone remodeling process. However, reconstructing large bone defects using CO₃Ap granules is difficult because of their granular shape. Therefore, we fabricated CO₃Ap honeycomb blocks (HCBs) with continuous unidirectional pores. We aimed to elucidate the tissue response and availability of CO₃Ap HCBs in the reconstruction of rabbit mandibular bone defects after marginal mandibulectomy. The percentages of the remaining CO₃Ap area and calcified bone area (newly formed bone) were estimated from the histological images. CO₃Ap area was 49.1 ± 4.9%, 30.3 ± 3.5%, and 25.5 ± 8.8%, whereas newly formed bone area was 3.0 ± 0.6%, 24.3 ± 3.3%, and 34.7 ± 4.8% at 4, 8, and 12 weeks, respectively, after implantation. Thus, CO₃Ap HCBs were gradually resorbed and replaced by new bone. The newly formed bone penetrated most of the pores in the CO₃Ap HCBs at 12 weeks after implantation. By contrast, the granulation tissue scarcely invaded the CO₃Ap HCBs. Some osteoclasts invaded the wall of CO₃Ap HCBs, making resorption pits. Furthermore, many osteoblasts were found on the newly formed bone, indicating ongoing bone remodeling. Blood vessels were also formed inside most of the pores in the CO₃Ap HCBs. These findings suggest that CO₃Ap HCBs have good osteoconductivity and can be used for the reconstruction of large mandibular bone defects.

Graphical abstract

The CO₃Ap HCB were gradually resorbed and replaced by newly formed bone.



Keywords Carbonate apatite · Bone substitute · Bone remodeling · Honeycomb blocks · Mandibular reconstruction

Supplementary information The online version contains supplementary material available at <https://doi.org/10.1007/s10856-022-06710-2>.

✉ Keiko Kudoh
kkudoh@tokushima-u.ac.jp

¹ Department of Oral Surgery, Institute of Biomedical Sciences, Tokushima University Graduate School, Tokushima, Japan

² Department of Biomaterials, Faculty of Dental Science, Kyushu University, Fukuoka, Japan

1 Introduction

The inorganic component of the human bone structure is not hydroxyapatite (HAp), but carbonate apatite (CO₃Ap). We had, therefore, attempted to and succeeded in fabricating low-crystalline CO₃Ap using a dissolution-precipitation reaction [1]. The CO₃Ap fabricated by the reaction was replaced with bone in phase with bone remodeling [2, 3]. Bone remodeling denotes the replacement of old bone with new bone through sequential osteoclastic resorption and

osteoblastic bone formation [4]. Unlike sintered hydroxyapatite (HAp), CO_3Ap can be resorbed by osteoclasts [3, 5, 6]. Bone replacement of CO_3Ap is thought to start from the resorption by osteoclasts in a manner similar to that of bone remodeling.

Kudoh et al. reported a first-in-human clinical trial of eight cases with one-stage sinus floor augmentation in which the CO_3Ap granules, fabricated by the reaction, led to adequate new bone formation to support dental implants that were maintained for 1 year, with no implant failures or complications [7]. Nakagawa et al. first reported 13 cases of two-stage sinus floor augmentation in which the CO_3Ap granules showed excellent biocompatibility and were replaced with bone in humans, as assessed via bone biopsy [8]. The survival and success rates of 17 implants after 3 years were 100%, with no corresponding complications [9]. Based on these clinical trials [7–9], the CO_3Ap granules were approved as an artificial bone substitute and marketed by GC Corporation as Cytrans Granules[®] in Japan and the United States. In Japan, no artificial bone substitutes had been previously approved for the reconstruction of bone defects adjacent to dental implants owing to their relatively poor osteoconductivity. CO_3Ap granules have been approved in all dental and maxillofacial fields, including those adjacent to dental implants, owing to their higher osteoconductivity.

The composition and structure of bone substitutes are the key factors governing their osteoconductivity and replacement of bone ability. Moreover, porous bone substitutes are useful because they allow bone tissues and blood vessels to penetrate the pores, leading to higher osteoconductivity and quicker bone regeneration [10, 11]. Furthermore, a porous surface improves the mechanical integrated bond between the bone substitute and the surrounding natural bone, providing greater mechanical stability [12, 13]. Therefore, CO_3Ap with porous structures is a promising bone substitute owing to its tendency to promote bone formation. Akita et al. succeeded in fabricating CO_3Ap granules with porous structures using microfibers [14]. Additionally, Ishikawa et al. fabricated porous CO_3Ap blocks with unidirectional continuous pores, called CO_3Ap honeycomb blocks (CO_3Ap HCBs) [15].

Bone defects in the oral and maxillofacial regions are caused by cancer resection, trauma, congenital malformations, progressive skeletal deformity, or orthognathic surgery. Bone reconstruction of specific regions is extremely difficult because of their complicated shapes. In the mandible, marginal or segmental mandibulectomy is performed for resecting odontogenic tumors (e.g., ameloblastoma), oral cancer, and mandibular osteomyelitis, including osteoradionecrosis and medication-related osteonecrosis of the jaw. Titanium reconstruction plates or autogenous bone grafts (e.g., from the fibula, scapula, iliac crest, or radial forearm osteocutaneous flap) are commonly used for the reconstruction of mandibular defects. Because titanium reconstruction plates are associated

with risks such as infection and exposure of the plate, screw loosening, and plate fracture, they are used for temporary mandibular reconstruction. Autogenous bone grafts are the gold standard for the reconstruction of mandibular defects, which can be vascularized, such as in the fibula flap, or non-vascularized, such as in the anterior and posterior iliac crest grafts [16]. Autogenous bone grafts demonstrate potential for contouring and immediate dental implant placement and exhibit bone regenerative ability. However, this technique has some disadvantages, such as the need for a healthy donor site surgery, long surgical time, high costs, complications, and long hospital stay. Therefore, the reconstruction of mandibular defects using an artificial bone substitute that is gradually replaced by natural bone is desirable. As mentioned above, CO_3Ap has excellent osteoconductive properties, biocompatibility, and the ability to be replaced with bone. In addition, the structure of CO_3Ap HCBs promotes bone penetration along the unidirectional continuous pores from both lateral ends. In other words, CO_3Ap HCBs might enable the reconstruction of large mandibular bone defects without autogenous bone grafting.

In this study, the tissue response and usefulness of CO_3Ap HCBs were evaluated for the reconstruction of rabbit mandibular bone defects caused by marginal mandibulectomy.

2 Materials and methods

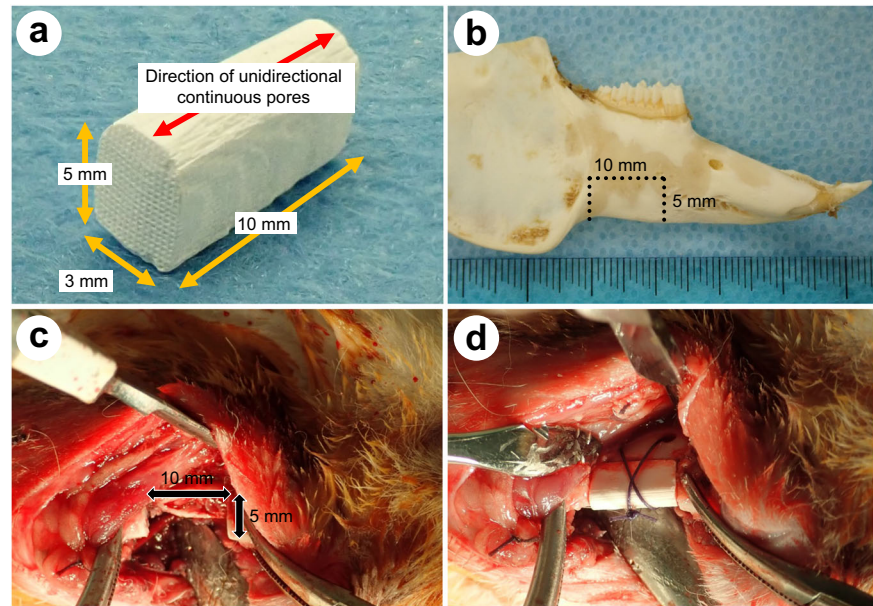
2.1 Materials

Calcium sulfate (CaSO_4) powder (purity >97%) was purchased from Nacalai Tesque (Kyoto, Japan) and heated to 700 °C for 6 h before use. The wax-based binder (catalog number: K18) was purchased from Nagamine Manufacturing Co., Ltd. (Manno-town, Japan).

2.2 Fabrication of CO_3Ap HCBs

CO_3Ap HCBs were prepared as previously described [17]. Briefly, CaSO_4 powder was mixed with a wax-based binder at 150 °C for 3 h using a Labo Plastomill M roller mixer (Toyo Seiki Co., Nagano, Japan) fitted with a uniaxial extruder. The mixture was extruded at 95 °C through a honeycomb (HC) extrusion die with 150 μm windows and a 300 μm pitch to generate HC rods. The HC rods were each cut to 2 cm in length to fabricate the blocks. The HCBs consisting of the binder containing CaSO_4 were heated to 900 °C in a box furnace and maintained for 24 h (Nitto Kagaku, Nagoya, Japan) to remove the binder. The CaSO_4 -containing HCBs were immersed in a mixture of 2 M NaHCO_3 and 2 M Na_2CO_3 and stored in a VTEC-18 incubator (Isuzu CAP, Niigata, Japan) at 40 °C for 4 days for conversion to CaCO_3 . The CaCO_3 HCBs were washed

Fig. 1 Application of the CO₃Ap HCBs for reconstruction of the rabbit mandibular bone defects. CO₃Ap HCB molded to a length, height, and width of 10, 5, and 3 mm, respectively (a). Excision image line of the rabbit mandibular defect (b). Inferior border osteotomy of the rabbit mandible (10 × 5 mm) (c). Grafting of the CO₃Ap HCBs to the bone defect (d)



multiple times with water, immersed in a 1 M Na₂HPO₄ solution, and stored in an incubator at 80 °C for 7 days for conversion to CO₃Ap. The CO₃Ap HCBs were subsequently rinsed with water several times.

2.3 Characterization of CO₃Ap HCBs

The CO₃Ap HCBs composition was determined using powder X-ray diffraction (XRD) analysis. Each sample was pulverized, and the XRD pattern was recorded using a D8 Advance diffractometer (Bruker AXS GmbH, Karlsruhe, Germany) with Cu K α radiation at 40 kV and 40 mA. The sample was scanned in continuous mode over a diffraction range of 20°–60° (2 θ).

The Fourier transform infrared (FT-IR) spectra were measured using a spectrometer (FT/IR-6200; JASCO, Tokyo, Japan) and the KBr disk method. The HCB structure was confirmed using stereomicroscopy and scanning electron microscopy (SEM) with S3400 N (Hitachi High Technologies, Tokyo, Japan). The acceleration voltage was set to 15 kV. Before analysis, the samples were coated with Au–Pd using an MSP-1S magnetron sputtering source (Vacuum Device Co., Ibaraki, Japan).

The carbonate content of the samples was measured using elemental analysis or a CHN coder (MT-6; Yanaco Analytical Instruments, Kyoto, Japan).

2.4 Application of the CO₃Ap HCBs for reconstruction of the rabbit mandibular bone defects

All animal experiments conformed to the guidelines of the Animal Ethics Committee of the Institute for Frontier

Medical Sciences, Tokushima University. Experimental protocols were reviewed and approved by the Tokushima University Animal Studies Committee (approval number: T30-46). Nine male Japanese white rabbits (body weight: 3.0–3.5 kg; SLC, Shizuoka, Japan) were used in this study. The rabbits were subjected to general anesthesia via intravenous injection of ketamine (10 mg kg⁻¹) and xylazine (3 mg kg⁻¹).

The skin of the buccal and lower sides of the mandible was shaved to remove the fur and was disinfected with a 10% povidone-iodine solution. After exposure of the mandibular body and ramus via the submandibular incision, 10 mm-long and 5 mm-deep bone defects were created using AESCULAP® ELAN EC (B. Braun Melsungen AG, Hessen, Germany) and a reciprocating saw. Each CO₃Ap HCB with a length of 10 mm, height of 5 mm, and width of 3 mm was implanted in each bone defect and fixed with surgical sutures (Fig. 1). The fasciae were then sutured. Inferior border osteotomy was performed bilaterally in each animal. Implantation of the HCB or an empty defect without an HCB was randomly performed. The rabbits were allowed unrestrained movement in their individual cages after recovery from anesthesia and a normal diet was provided.

2.5 Microcomputed tomography (μ -CT)

The animals were euthanized via intravenous injection of pentobarbital (120 mg kg⁻¹), and the mandibular bone was harvested at 4, 8, and 12 weeks after the operation. The excised mandibular bone was scanned using μ -CT with SkyScan1176 (Bruker microCT, Kontich, Belgium) at a source voltage and current of 50 kV and 500 μ A,

respectively. The image data were recreated using the NRecon Reconstruction software (Bruker microCT). Bone formation in the defects, including the specimens, was observed.

2.6 Histological evaluation

Three samples from each group were fixed in 10% buffer formaldehyde for 7 days and dehydrated by immersion in graded ethanol solutions (from 70% to 100%). Finally, the samples were embedded in methyl methacrylate (WAKO Pure Chemical Corporation, Osaka, Japan). Sections were prepared for pathological analysis using a modified interlocked diamond saw (Exakt, Hamburg, Germany), and Villanueva Goldner stain was applied to all sections. All specimens were observed using an all-in-one microscope (BZ-X700; KEYENCE, Osaka, Japan).

To clarify the elongation of newly formed bone from the lateral parts at both ends of the bone defect, the defect area was divided into three parts: the central part and the lateral parts at both ends (Fig. 2). The percentage of newly formed bone (calcified bone stained in green) area in the defect was calculated using the ImageJ software (version 1.53a, Wayne Rasband, National Institutes of Health, USA). Furthermore, the percentage of the remaining CO₃Ap area was calculated using the same method.

2.7 Statistical analysis

For statistical analysis, one-way factorial analysis of variance and Fisher's least significant difference *post-hoc* tests were performed using Kaleida Graph (version 4.1, Hulinks, Tokyo, Japan). Values are expressed as mean \pm SD. Statistical significance was set at $p < 0.05$.

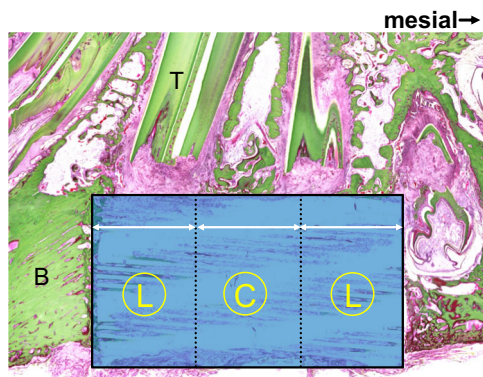


Fig. 2 Compartments for the microscopic analysis of regenerated bone and residual CO₃Ap in the defects. The right direction of the figure shows the mesial aspect. Specimens were divided into three parts, that is, the central part (C) and the lateral parts at both ends (L). “B” indicates the cortical bone of the inferior border of the mandible. “T” indicates tooth

3 Results

3.1 Compositional and morphologic analysis

Figure 3 shows stereomicroscopy (Fig. 3a) and SEM (Fig. 3b, c) images of CO₃Ap HCBs. The CO₃Ap HCBs exhibited a typical HC structure. In other words, the HCBs comprised square through-holes extending in one direction. The length of the macropore square side was $129 \pm 6 \mu\text{m}$, and the thickness of the strut was $130 \pm 5 \mu\text{m}$ (Fig. 3b). A high-magnification image showed that the CO₃Ap HCBs consisted of small crystallites that were mutually interlocked (Fig. 3c).

Figure 4 summarizes the XRD patterns of the CO₃Ap HCBs, Cytrans Granules[®] (CO₃Ap granules), and HAp standard substance (STD). All samples demonstrated apatitic patterns characteristic of an apatite crystalline phase. The HAp STD showed sharp peaks that indicated high crystallinity, whereas the CO₃Ap HCBs and Cytrans Granules[®] showed broader peaks, suggesting low crystallinity.

The FT-IR spectra of the CO₃Ap HCB, Cytrans Granules[®], and HAp STD are shown in Fig. 5. Absorption attributed to CO₃²⁻ (\blacktriangle) in B-type CO₃Ap was observed at 1455, 1440, and 875 cm⁻¹ for the CO₃Ap HCBs and Cytrans Granules[®], whereas no such absorption was observed for the HAp STD. By contrast, absorption attributed to OH⁻ (\triangle) was observed at 3568 and 627 cm⁻¹ for the HAp STD, whereas no such absorption was observed for the CO₃Ap HCBs. CO₃Ap HCBs and Cytrans Granules[®] showed almost the same XRD pattern and FT-IR spectra.

The carbonate content of the CO₃Ap HCB was 11.1% \pm 1.2%, almost identical to that of the Cytrans Granules[®] (11.8 \pm 0.6%) [7].

3.2 Imaging analysis

Figure 6 shows typical μ -CT images of an empty defect and a CO₃Ap HCB at day 0 (immediately after implantation), and 4, 8, and 12 weeks after implantation. With no reconstruction (Fig. 6a–c), no continuity of the inferior border of the mandibular bone was observed during the observation period, indicating that this defect was a critical size defect and had cured with a hollow border. By contrast, when the defect was reconstructed with the CO₃Ap HCB, the continuity of the inferior border of the mandibular bone was repaired, as assessed in the implantation samples (Fig. 6e–g). Modest resorption of the CO₃Ap HCB was observed 4 weeks after implantation (Fig. 6e). At 8 and 12 weeks after implantation, the resorption of the CO₃Ap HCB progressed with time, although the implanted HCB remained in place and retained the HC structure (Fig. 6f, g).

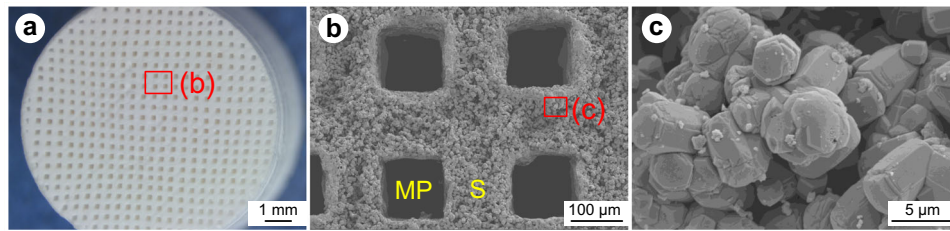


Fig. 3 Stereomicroscopy and SEM images of CO₃Ap HCBs. Stereomicroscopy image of a CO₃Ap HCB (a). SEM image of a CO₃Ap HCB (b, c). “S” and “MP” indicate a honeycomb strut and macropore, respectively. Magnified SEM images of the struts of the CO₃Ap HCB (c)

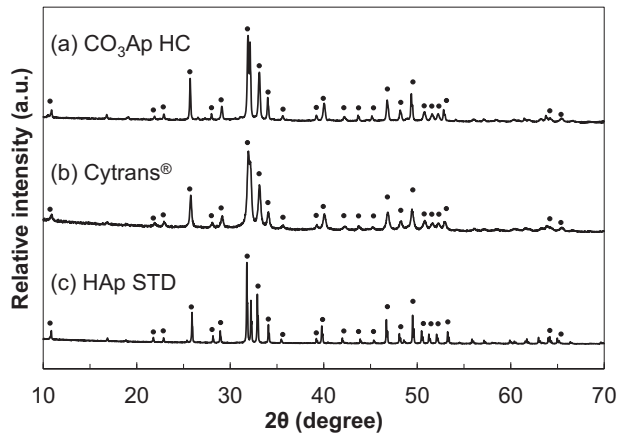


Fig. 4 XRD patterns. CO₃Ap HCBs (HC) (a), Cytrans Granules® (Cytrans®; CO₃Ap granules) (b), and HAp standard substance (STD) (c). Circles indicate the apatite diffraction peaks

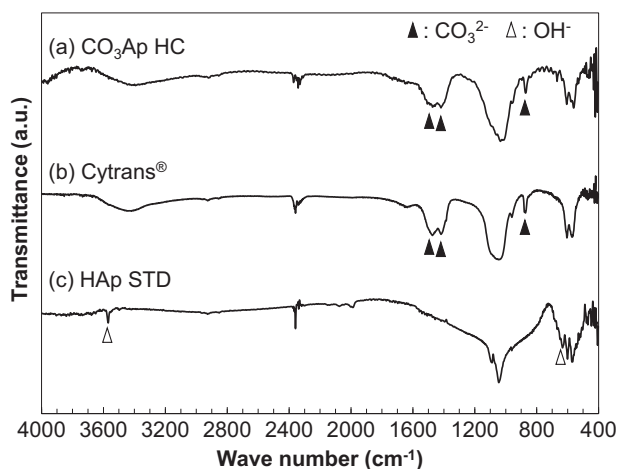


Fig. 5 FT-IR spectra. CO₃Ap HCBs (HC) (a), Cytrans Granules® (Cytrans®; CO₃Ap granules) (b), and HAp standard substance (STD) (c). Black triangles correspond to the B-type CO₃²⁻ peaks (1455, 1410, and 875 cm⁻¹)

The cross-sections obtained 4 and 8 weeks after implantation showed that the mineral bonelike structure contiguous to the bone defect end was visible at the outside of the HCB (Fig. 6i, j). At 12 weeks after implantation, the mineral

bonelike structure completely surrounded the HCB (Fig. 6k).

3.3 Histological analysis

Figure 7 shows typical histological images with Villanueva Goldner staining of the CO₃Ap HCBs 4, 8, and 12 weeks after reconstruction. Few inflammatory cells or foreign body giant cells were observed regardless of the period after reconstruction. The resorption of CO₃Ap HCBs was observed and radiographical evaluation was performed using the μ -CT images (Fig. 7a–c). Only modest resorption of CO₃Ap HCBs occurred 4 weeks after reconstruction (Fig. 7a). At 8 and 12 weeks after reconstruction, the partial resorption of the CO₃Ap HCBs progressed with time, although the HCBs remained in place and retained the HC structure (Fig. 7b, c). At 4 weeks after reconstruction, the bone extending from the existing bone was in contact with the lateral ends of the CO₃Ap HCB, and a small amount of bone was observed in unidirectional continuous pores of the lateral parts at both ends but not in the central part of the CO₃Ap HCB (Fig. 7a, d, g). At 8 and 12 weeks after reconstruction, calcified bone was observed in the pores of the lateral parts at both ends and in the central part of CO₃Ap HCBs (Fig. 7b, c, e, f, h, and i). Furthermore, cross-linked structures of the bone between neighbor continuous pores were observed 12 weeks after reconstruction (Fig. 7i).

High-magnification images showed new bone formation along the continuous pores of CO₃Ap HCBs (Fig. 8). Some osteoclasts invaded the wall of CO₃Ap HCBs, forming resorption pits 4 weeks after implantation (Fig. 8a). In the neighboring environment, osteoblasts formed new bone (Fig. 8a). The thickness of which increased over time (Fig. 8b, c). Many osteoblasts were observed on the surface of the newly formed bone, and osteocytes were observed within the bone matrix. Numerous vascular endothelial cells and red blood cells were also found inside most of the pores, indicating the formation of blood vessels. Additionally, few inflammatory cells or foreign body giant cells were observed in the pores.

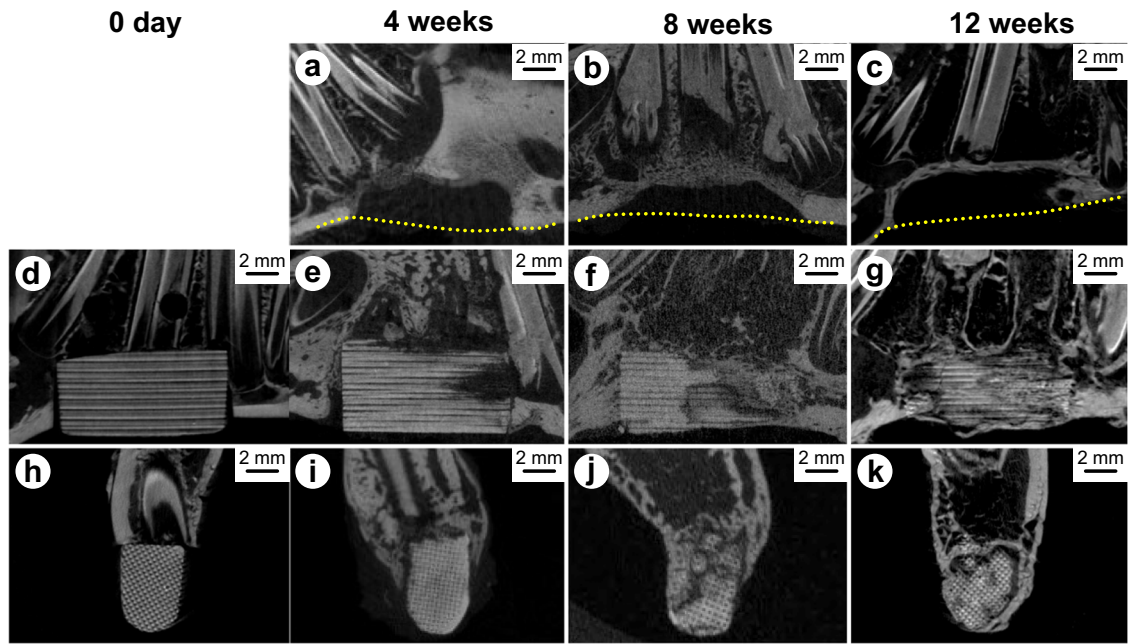


Fig. 6 μ -CT images. The empty defect (a–c) and CO₃Ap HCB (d–k) at day 0 (immediately after implantation) and 4, 8, and 12 weeks after implantation. The dotted lines (a–c) show the removed mandibular border. Sagittal sections (a–g) and cross-sections (h–k) of the pores

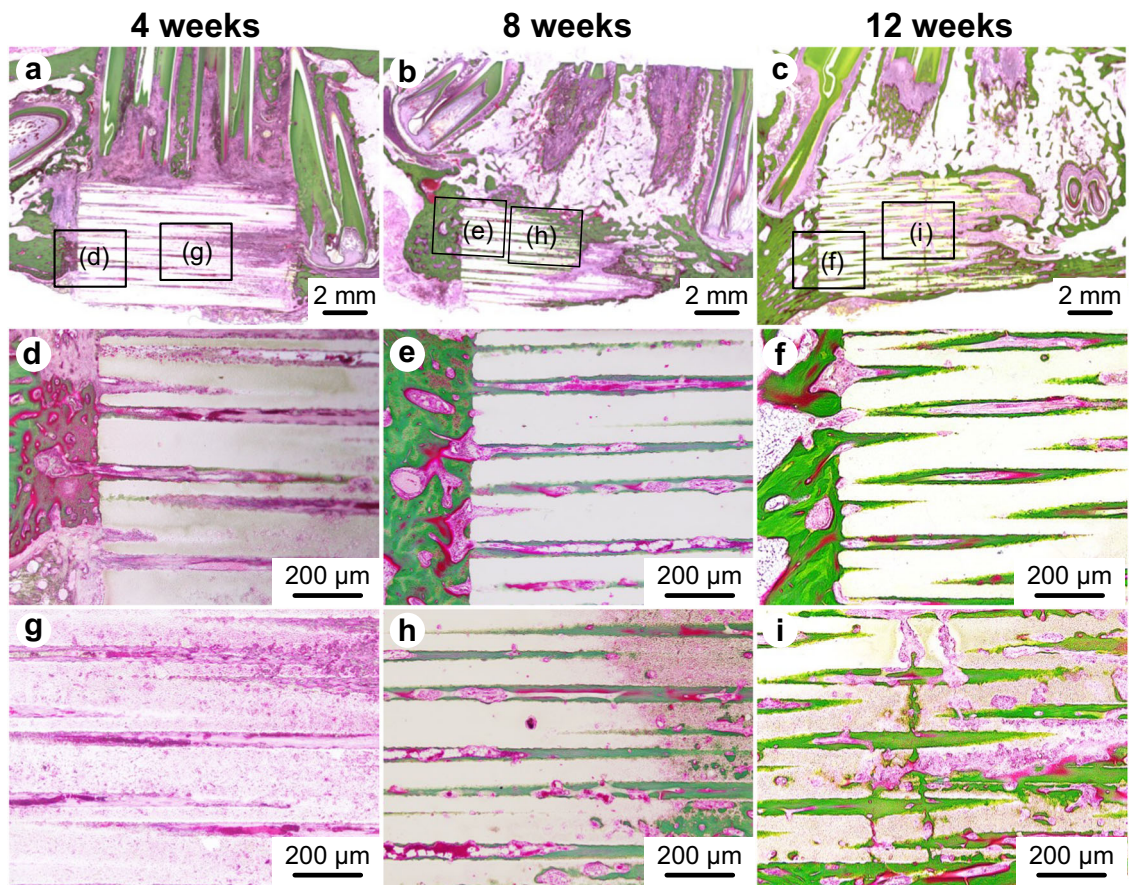


Fig. 7 Typical histological images resulting from Villanueva Goldner staining of CO₃Ap HCBs. At 4 (a, d, g), 8 (b, e, h), and 12 weeks (c, f, i) after implantation

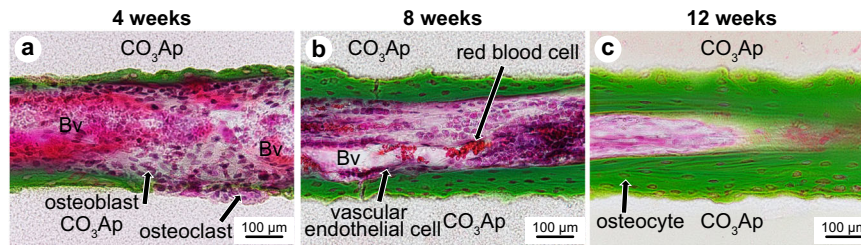
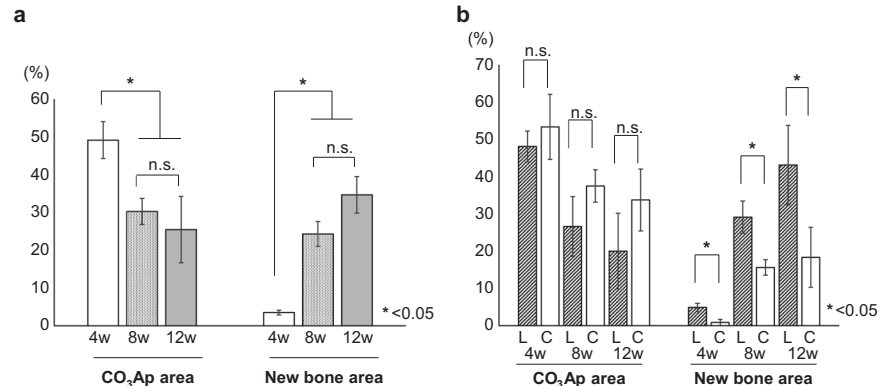


Fig. 8 High-magnification images displaying the Villanueva Goldner staining of CO₃Ap HCBs. At 4 (a), 8 (b), and 12 weeks (c) after implantation. Blood vessels (Bv) were found in the pores of CO₃Ap

HCBs. New bone was formed along the pores of the CO₃Ap HCB and the thickness of the new bone increased over time

Fig. 9 Comparison of new bone area and residual CO₃Ap area. Percentage of new bone and residual CO₃Ap 2, 4, and 8 weeks after implantation (a). **p* < 0.05. Percentage of new bone and residual CO₃Ap 2, 4, and 8 weeks after implantation in the central part (C) and in the lateral parts at both ends (L) (b). **p* < 0.05



The percentages of the remaining CO₃Ap area and calcified bone area (newly formed bone) stained green were estimated from the histological images (Fig. 9a). The CO₃Ap area decreased over time. The calcified bone area stained in green increased with time. The following results at 4, 8, and 12 weeks after implantation were obtained (in%): CO₃Ap area was 49.1 ± 4.9, 30.3 ± 3.5, and 25.5 ± 8.8, whereas calcified bone area stained in green was 3.0 ± 0.6, 24.3 ± 3.3, and 34.7 ± 4.8, respectively.

In addition, the percentages of the remaining CO₃Ap area and calcified bone area stained green were estimated by dividing them into three parts: the lateral parts at both ends and the central part (Fig. 9b), and the following results at 4, 8, and 12 weeks after reconstruction (in%) were obtained: CO₃Ap area in the lateral parts at both ends was 48.1 ± 4.1, 26.6 ± 8.0, and 20.0 ± 10.2, whereas CO₃Ap area in the central part was 53.3 ± 8.7, 37.5 ± 4.3, and 33.7 ± 8.3; calcified bone area stained green in the lateral parts at both ends was 4.9 ± 1.1, 29.1 ± 4.3, and 43.1 ± 10.6; and calcified bone area stained green in the central part was 0.9 ± 0.9, 15.6 ± 2.1, and 18.3 ± 8.1, respectively.

4 Discussion

Our results demonstrate that CO₃Ap HCBs promote bone penetration along the unidirectional continuous pores from both lateral ends. The CO₃Ap HCBs could restore the

continuity of the bone in a 1 cm-long rabbit mandibular marginal bone defect. The CO₃Ap HCBs showed excellent tissue response and good osteoconductivity and promoted the penetration of not only bone tissue but also blood vessels.

Ogose et al. reported that HAp is not resorbed and is entirely retained in human bone defects for periods longer than 130 months after implantation [18]. Furthermore, Hayashi et al. reported that HAp HCs are hardly resorbed at 12 weeks after implantation [19]. By contrast, beta-tricalcium phosphate (β-TCP) spontaneously dissolves under physiological conditions and in the absence of osteoclastic resorption [20, 21]. The β-TCP HCB is resorbed extremely rapidly and only a small amount remains 12 weeks after implantation [19].

Doi et al. reported that cultured osteoclasts resorb sintered CO₃Ap disks [20]. CO₃Ap is resorbed only via osteoclastic resorption, and its resorption rate and degree are similar to those of natural bone minerals [20–22]. Ishikawa et al. also reported that a CO₃Ap HCBs are resorbed by osteoclasts and replaced with bone in rabbit femoral bone defects [15, 19]. The difference in resorption between CO₃Ap and HAp was attributed to the presence of carbonate and the low crystallinity of CO₃Ap. Spence et al. reported that a high carbonate content in carbonate-substituted hydroxyapatite (CHA) leads to increased osteoclastogenesis in culture and that the resorption of CHA increases with an increasing carbonate content [23]. Human bones contain 11% ± 1% of carbonate ions [24]. In the present study, the

carbonate content of the CO₃Ap HCB was set to be nearly equal to that of a human bone, and the results of CHN elemental analysis showed that the carbonate content of the CO₃Ap HCB was 11.1% ± 1.2%.

The pores of biomaterials allow the passage of cells, delivery of oxygen and nutrients from the blood vessels, and removal of waste [25–27]. The pore size must be carefully controlled to improve the efficacy of bone regeneration [28, 29]. The optimum pore size for bone infiltration is debatable and depends on biomaterials such as titanium and calcium phosphate [13, 25, 30]. Frosch et al. and Taniguchi et al. reported that porous titanium implants with a pore size of approximately 600 µm are suitable for bone formation [31, 32].

HAp and β-TCP are representative calcium phosphates that are used as bone substitutes. Chang et al. reported bone ingrowth in porous HAp implants with different pore sizes (50, 100, 300, and 500 µm) in the proximal tibia of rabbits and concluded that the 300 µm pores in the HAp implants are of optimal size [33]. Kuboki et al. reported that the alkaline phosphatase activity and osteocalcin content are higher in bone morphogenetic protein-containing porous HAp blocks with a pore size of 300–400 µm than in those with different pore sizes (106–212, 212–300, 400–500, and 500–600 µm) when implanted subcutaneously in rats [34]. Moreover, infiltration of capillaries was observed in the porous HAp blocks with pore sizes greater than 300 µm. Taking these reports into consideration, a pore size ranging from 300 to 400 µm appears to be optimal for porous HAp.

Diao et al. studied biodegradable bone substrates, β-TCP scaffolds with a pore size of 100, 250, and 400 µm, in calvarial defects of rats at 4 weeks [35]. The use of porous β-TCP scaffolds with a pore size of 100 µm enabled a higher percentage of new bone ingrowth than the use of scaffolds with other pore sizes (250 and 400 µm); the porous β-TCP scaffolds with pores of both 250 and 400 µm were occupied by a larger amount of fibrous tissue [36]. A pore size of 100 µm appears to be optimal for porous β-TCP.

Akita et al. also reported a similar phenomenon in porous CO₃Ap granules [14]. CO₃Ap granules with a pore size of 120 µm showed the highest new bone formation inside the pores during the early stages among the various pore sizes (30, 50, 120, and 205 µm) [14]. Moreover, even though the pores sizes of 30, 50, and 120 µm were occupied by bone, fibrous tissue occupied the 205 µm pores of CO₃Ap. Hence, it was suggested that the optimum pore size of CO₃Ap is approximately 120 µm, which is smaller than that of HAp. By contrast, Hayashi et al. reported that bone formation in the pores of the CO₃Ap HCB (macropores of 300 µm) is significantly superior to that in the 100 and 200 µm pores [36]. Thus, it was claimed that the effective pore size of the CO₃Ap HCB for bone regeneration is between 200 and 300 µm, which is larger than that reported by Akita et al. [14]. The

optimum pore size of CO₃Ap for bone penetration remains controversial. The difference between the results of Akita et al. and Hayashi et al. could be attributed to the following three points: the CO₃Ap HCB raw materials, the sectional shape of the pores, and the CO₃Ap shape. The CO₃Ap reported by Hayashi et al. was made from calcium hydroxide (Ca(OH)₂), whereas that reported by Akita et al. and our team was made from CaSO₄. In terms of sectional shape, square-shaped pores were found in the study by Hayashi et al. and in our study, whereas circular pores were found in the study by Akita et al. In the study by Hayashi et al. as well as in this study, the CO₃Ap had a block shape (dimensions of approximately 5–10 mm); however, in the study by Akita et al., CO₃Ap had a porous granule shape (dimensions of approximately 1–2 mm). More studies are needed to determine the optimal pore size of the CO₃Ap HCBs.

In this study, CO₃Ap area decreased with time: 49.1 ± 4.9, 30.3 ± 3.5, and 25.5 ± 8.8% at 4, 8, and 12 weeks after implantation, respectively. By contrast, calcified bone area stained in green increased: 3.0 ± 0.6, 24.3 ± 3.3, and 34.7 ± 4.8% at 4, 8, and 12 weeks after implantation, respectively. In short, CO₃Ap HCBs were gradually resorbed and replaced by newly formed bone. New bone was formed even in the central part of the 1 cm CO₃Ap HCB at 8 and 12 weeks after implantation. Moreover, in high-magnification images, some osteoclasts were observed to resorb the wall of CO₃Ap HCBs, and osteoblasts also formed new bone in the neighboring environment at 4 weeks after implantation. This suggests that replacement of CO₃Ap HCBs starts from osteoclast resorption in a manner similar to that of the bone remodeling.

Nagai et al. reported that cultured human bone marrow cells on CO₃Ap disks promote osteoblastic differentiation earlier than when cultured on HAp disks, after 7 days of culture [2]. Ishikawa et al. reported that CO₃Ap (Cytrans Granules[®]) histologically elicits a larger amount of new bone formation than HAp (Neobone[®], CoorsTec, Tokyo, Japan) and β-TCP (Cerasorb[®], Hakuho, Tokyo, Japan) in a hybrid dog mandible bone defect model 4 and 12 weeks after implantation [37]. Hayashi et al. reported that bone maturation is faster in the CO₃Ap HCBs than in the HAp and β-TCP HCBs, and the amount of bone formation was higher in the CO₃Ap HCBs than in the HAp and β-TCP HCBs in a rabbit rear limb defect model 4 and 12 weeks after implantation [19]. These results demonstrate that CO₃Ap exhibits higher osteoconductivity than HAp and β-TCP.

Moreover, the structure of the HCBs has two merits for bone regeneration: 1) it can provide the space (continuous unidirectional pore) where new bone is formed and promote the infiltration of the bone from both lateral ends; 2) the wall of the pore can block the invasion of the soft tissue from the lateral sides. Consequently, more time is granted

for bone infiltration and regeneration in the pores. Therefore, the CO₃Ap HCB has an excellent ability to reconstruct relatively widespread bone defects caused by marginal mandibulectomy.

Substantial compressive strength that can withstand occlusal force is needed as a characteristic of reconstruction materials for mandibular bone defects. Misch et al. reported that the ultimate compressive strength of the trabecular bone in the human mandible ranges from 0.22 to 10.44 MPa, with a mean value of 3.9 MPa [38]. In the present study, the CO₃Ap HCB was able to retain its form as a reconstructing material in the rabbit mandibular bone defect made via inferior border mandibulectomy during the observation period of 12 weeks. Regenos® (Kuraray Co., Tokyo, Japan) is a commercial HAp artificial bone with unidirectional macroporous structures similar to those of the CO₃Ap HCB. The compressive strength of Regenos® and the CO₃Ap HCB is 14 MPa and 22.8 ± 3.5 MPa, respectively [19, 39]. In other words, the compressive strength of Regenos® is considerably lower than that of the CO₃Ap HCB. The straight struts present in the CO₃Ap HCBs are separate, whereas the struts in Regenos® are not completely straight and lean against each other. Orientation, linearity, and independence are critical in increasing the compressive strength along the macropores while maintaining a high porosity. Therefore, the CO₃Ap HCBs structure seems to be an optimal structure because it possesses both high mechanical strength and high porosity.

Regenos® is widely used in the orthopedic field in Japan for bone defects of the arm, leg, and vertebra, bearing large loads [40, 41]. It has already been applied in clinical cases to intra-articular calcaneal fractures with large bone defects and distal radius fractures and has yielded good results [42, 43]. The CO₃Ap HCB has sufficient potential for clinical use in dental and orthopedic fields because it has higher compressive strength and osteoconductivity than Regenos®, which is composed of HAp. In the near future, we aim to further investigate the applicability of the CO₃Ap HCBs in the treatment of larger bone defects, such as segmental mandibulectomy, with longer observation periods to assess its clinical use.

5 Conclusions

This study is the first to report on the reconstruction of rabbit mandibular bone defects using the CO₃Ap HCBs fabricated using the extrusion technique. The CO₃Ap HCBs were gradually resorbed and replaced by newly formed bone. The morphology of CO₃Ap HCBs not only promotes the bone infiltration from both lateral ends, but also inhibits the invasion of soft tissue from the lateral sides. The CO₃Ap HCBs were found to have the capability to restore the

continuity of 1-cm-long rabbit mandibular marginal bone defects. CO₃Ap HCBs showed an excellent tissue response and good osteoconductivity and may be useful in the reconstruction of large mandibular bone defects.

Acknowledgements This research was supported partially by AMED [grant number 19im0502004h0208] and JSPS KAKENHI [grant number JP20K10180].

Author contributions KK: Conceptualization, Methodology, Data curation, Funding acquisition, Validation, Visualization, and Writing-review & editing. NF: Methodology, Investigation, Validation, and Editing. KA: Methodology, Formal analysis, Investigation, and Editing. TK: Formal analysis, Investigation, and Software. NT: Investigation and Editing. NK: Investigation and Editing. KH: Methodology and Resources. KI: Funding acquisition, Methodology, Resources, and Writing-review & editing. YM: Project administration, Supervision, and Writing-review & editing. All authors critically revised the report, commented on drafts of the manuscript, and approved the final report.

Compliance with ethical standards

Conflict of interest The authors declare no competing interests.

Ethical approval All animal experiments conformed to the guidelines of the Animal Ethics Committee of the Institute for Frontier Medical Sciences, Tokushima University. Experimental protocols were reviewed and approved by the Tokushima University Animal Studies Committee (approval number: T30-46).

Publisher's note Springer Nature remains neutral with regard to jurisdictional claims in published maps and institutional affiliations.

Open Access This article is licensed under a Creative Commons Attribution 4.0 International License, which permits use, sharing, adaptation, distribution and reproduction in any medium or format, as long as you give appropriate credit to the original author(s) and the source, provide a link to the Creative Commons license, and indicate if changes were made. The images or other third party material in this article are included in the article's Creative Commons license, unless indicated otherwise in a credit line to the material. If material is not included in the article's Creative Commons license and your intended use is not permitted by statutory regulation or exceeds the permitted use, you will need to obtain permission directly from the copyright holder. To view a copy of this license, visit <http://creativecommons.org/licenses/by/4.0/>.

References

- Ishikawa K, Matsuya S, Lin X, Lei Z, Yuasa T, Miyamoto Y. Fabrication of low crystalline B-type carbonate apatite block from low crystalline calcite block. *J Ceram Soc Jpn*. 2010;118:341–4. <https://doi.org/10.2109/jcersj2.118.341>
- Nagai H, Kobayashi-Fujioka M, Fujisawa K, Ohe G, Takamaru N, Hara K, et al. Effects of low crystalline carbonate apatite on proliferation and osteoblastic differentiation of human bone marrow cells. *J Mater Sci Mater Med*. 2015;26:99. <https://doi.org/10.1007/s10856-015-5431-5>
- Fujisawa K, Akita K, Fukuda N, Kamada K, Kudoh T, Ohe G, et al. Compositional and histological comparison of carbonate apatite fabricated by dissolution–precipitation reaction and Bio-

- Oss[®]. *J Mater Sci Mater Med*. 2018;29:121. <https://doi.org/10.1007/s10856-018-6129-2>
4. Kenkre JS, Bassett J. The bone remodelling cycle. *Ann Clin Biochem*. 2018;55:308–27. <https://doi.org/10.1177/0004563218759371>
 5. Ishikawa K, Hayashi K. Carbonate apatite artificial bone. *Sci Technol Adv Mater*. 2021;22:683–94. <https://doi.org/10.1080/14686996.2021.1947120>
 6. Fujioka-Kobayashi M, Miyamoto Y, Ishikawa K, Satomi T, Schaller B. Osteoclast behaviors on the surface of deproteinized bovine bone mineral and carbonate apatite substitutes in vitro. *J Biomed Mater Res A*. 2022;110:1524–32. <https://doi.org/10.1002/jbm.a.37392>
 7. Kudoh K, Fukuda N, Kasugai S, Tachikawa N, Koyano K, Matsushita Y, et al. Maxillary sinus floor augmentation using low-crystalline carbonate apatite granules with simultaneous implant installation: first-in-human clinical trial. *J Oral Maxillofac Surg*. 2019;77:985.e1–985.e11. <https://doi.org/10.1016/j.joms.2018.11.026>
 8. Nakagawa T, Kudoh K, Fukuda N, Kasugai S, Tachikawa N, Koyano K, et al. Application of low-crystalline carbonate apatite granules in 2-stage sinus floor augmentation: a prospective clinical trial and histomorphometric evaluation. *J Periodontol Implant Sci*. 2019;49:382–96. <https://doi.org/10.5051/jpis.2019.49.6.382>
 9. Ogino Y, Ayukawa Y, Tachikawa N, Shimogishi M, Miyamoto Y, Kudoh K, et al. Staged sinus floor elevation using novel low-crystalline carbonate apatite granules: prospective results after 3-year functional loading. *Mater (Basel)*. 2021;14:5760. <https://doi.org/10.3390/ma14195760>
 10. Ishikawa K, Arifita TI, Hayashi K, Tsuru K. Fabrication and evaluation of interconnected porous carbonate apatite from alpha tricalcium phosphate spheres. *J Biomed Mater Res B Appl Biomater*. 2019;107:269–77. <https://doi.org/10.1002/jbm.b.34117>
 11. Zhao YN, Fan JJ, Li ZQ, Liu YW, Wu YP, Liu J. Effects of pore size on the osteoconductivity and mechanical properties of calcium phosphate cement in a rabbit model. *Artif Organs*. 2017;41:199–204. <https://doi.org/10.1111/aor.12742>
 12. Hannink G, Arts JJC. Bioresorbability, porosity and mechanical strength of bone substitutes: what is optimal for bone regeneration. *Injury*. 2011;42:S22–5. <https://doi.org/10.1016/j.injury.2011.06.008>
 13. Karageorgiou V, Kaplan D. Porosity of 3D biomaterial scaffolds and osteogenesis. *Biomaterials*. 2005;26:5474–91. <https://doi.org/10.1016/j.biomaterials.2005.02.002>
 14. Akita K, Fukuda N, Kamada K, Kudoh K, Kurio N, Tsuru K, et al. Fabrication of porous carbonate apatite granules using microfiber and its histological evaluations in rabbit calvarial bone defects. *J Biomed Mater Res A*. 2020;108:709–21. <https://doi.org/10.1002/jbm.a.36850>
 15. Ishikawa K, Munar ML, Tsuru K, Miyamoto Y. Fabrication of carbonate apatite honeycomb and its tissue response. *J Biomed Mater Res A*. 2019;107:1014–20. <https://doi.org/10.1002/jbm.a.36640>
 16. Marechek A, AlShare A, Pack S, Demko C, Quereshey FA, Baur D. Nonvascularized bone grafts for reconstruction of segmental mandibular defects: is length of graft a factor of success. *J Oral Maxillofac Surg*. 2019;77:2557–66. <https://doi.org/10.1016/j.joms.2019.05.008>
 17. Hayashi K, Kishida R, Tsuchiya A, Ishikawa K. Carbonate apatite micro-honeycombed blocks generate bone marrow-like tissues as well as bone. *Adv Biosyst*. 2019;3:e1900140. <https://doi.org/10.1002/adbi.201900140>
 18. Ogose A, Hotta T, Kawashima H, Kondo N, Gu W, Kamura T, et al. Comparison of hydroxyapatite and beta tricalcium phosphate as bone substitutes after excision of bone tumors. *J Biomed Mater Res B Appl Biomater*. 2005;72:94–101. <https://doi.org/10.1002/jbm.b.30136>
 19. Hayashi K, Kishida R, Tsuchiya A, Ishikawa K. Honeycomb blocks composed of carbonate apatite, β -tricalcium phosphate, and hydroxyapatite for bone regeneration: effects of composition on biological responses. *Mater Today Bio*. 2019;4:100031. <https://doi.org/10.1016/j.mtbio.2019.100031>
 20. Doi Y, Iwanaga H, Shibutani T, Moriwaki Y, Iwayama Y. Osteoclastic responses to various calcium phosphates in cell cultures. *J Biomed Mater Res*. 1999;47:424–33. 10.1002/(sici)1097-4636(19991205)47:3<424::aid-jbm19>3.0.co;2-0
 21. Yamasaki N, Hirao M, Nanno K, Sugiyasu K, Tamai N, Hashimoto N, et al. A comparative assessment of synthetic ceramic bone substitutes with different composition and microstructure in rabbit femoral condyle model. *J Biomed Mater Res B Appl Biomater*. 2009;91:788–98. <https://doi.org/10.1002/jbm.b.31457>
 22. Hasegawa M, Doi Y, Uchida A. Cell-mediated bioresorption of sintered carbonate apatite in rabbits. *J Bone Jt Surg Br*. 2003;85:142–7. <https://doi.org/10.1302/0301-620x.85b1.13414>
 23. Spence G, Patel N, Brooks R, Bonfield W, Rushton N. Osteoclastogenesis on hydroxyapatite ceramics: the effect of carbonate substitution. *J Biomed Mater Res A*. 2010;92:1292–300. <https://doi.org/10.1002/jbm.a.32373>
 24. Elliott JC, Holcomb DW, Young RA. Infrared determination of the degree of substitution of hydroxyl by carbonate ions in human dental enamel. *Calcif Tissue Int*. 1985;37:372–5. <https://doi.org/10.1007/BF02553704>
 25. Bobbert FSL, Zadpoor AA. Effects of bone substitute architecture and surface properties on cell response, angiogenesis, and structure of new bone. *J Mater Chem B*. 2017;5:6175–92. <https://doi.org/10.1039/c7tb00741h>
 26. Codogno P, Meijer AJ. Autophagy and signaling: their role in cell survival and cell death. *Cell Death Differ*. 2005;12(Suppl 2):1509–18. <https://doi.org/10.1038/sj.cdd.4401751>
 27. Kim SS, Utsunomiya H, Koski JA, Wu BM, Cima MJ, Sohn J, et al. Survival and function of hepatocytes on a novel three-dimensional synthetic biodegradable polymer scaffold with an intrinsic network of channels. *Ann Surg*. 1998;228:8–13. <https://doi.org/10.1097/0000658-199807000-00002>
 28. Bohner M, Loosli Y, Baroud G, Lacroix D. Commentary: deciphering the link between architecture and biological response of a bone graft substitute. *Acta Biomater*. 2011;7:478–84. <https://doi.org/10.1016/j.actbio.2010.08.008>
 29. Dias MR, Fernandes PR, Guedes JM, Hollister SJ. Permeability analysis of scaffolds for bone tissue engineering. *J Biomech*. 2012;45:938–44. <https://doi.org/10.1016/j.jbiomech.2012.01.019>
 30. Bharadwaz A, Jayasuriya AC. Recent trends in the application of widely used natural and synthetic polymer nanocomposites in bone tissue regeneration. *Mater Sci Eng C Mater Biol Appl*. 2020;110:110698. <https://doi.org/10.1016/j.msec.2020.110698>
 31. Frosch KH, Barvencik F, Viereck V, Lohmann CH, Dresing K, Breme J, et al. Growth behavior, matrix production, and gene expression of human osteoblasts in defined cylindrical titanium channels. *J Biomed Mater Res A*. 2004;68:325–34. <https://doi.org/10.1002/jbm.a.20010>
 32. Taniguchi N, Fujibayashi S, Takemoto M, Sasaki K, Otsuki B, Nakamura T, et al. Effect of pore size on bone ingrowth into porous titanium implants fabricated by additive manufacturing: an in vivo experiment. *Mater Sci Eng C Mater Biol Appl*. 2016;59:690–701. <https://doi.org/10.1016/j.msec.2015.10.069>
 33. Chang BS, Lee CK, Hong KS, Youn HJ, Ryu HS, Chung SS, et al. Osteoconduction at porous hydroxyapatite with various pore configurations. *Biomaterials*. 2000;21:1291–8. [https://doi.org/10.1016/S0142-9612\(00\)00030-2](https://doi.org/10.1016/S0142-9612(00)00030-2)
 34. Kuboki Y, Jin Q, Takita H. Geometry of carriers controlling phenotypic expression in BMP-induced osteogenesis and chondrogenesis. *J Bone Jt Surg Am*. 2001;83-A:S105–15. <https://doi.org/10.2106/00004623-200100002-00005>
 35. Diao J, OuYang JO, Deng T, Liu X, Feng Y, Zhao N, et al. 3D-plotted beta-tricalcium phosphate scaffolds with smaller pore sizes

- improve in vivo bone regeneration and biomechanical properties in a critical-sized calvarial defect rat model. *Adv Health Mater.* 2018;7:e1800441. <https://doi.org/10.1002/adhm.201800441>
36. Hayashi K, Munar ML, Ishikawa K. Effects of macropore size in carbonate apatite honeycomb scaffolds on bone regeneration. *Mater Sci Eng C Mater Biol Appl.* 2020;111:110848. <https://doi.org/10.1016/j.msec.2020.110848>
37. Ishikawa K, Miyamoto Y, Tsuchiya A, Hayashi K, Tsuru K, Ohe G. Physical and histological comparison of hydroxyapatite, carbonate apatite, and β -tricalcium phosphate bone substitutes. *Mater (Basel).* 2018;11:1993. <https://doi.org/10.3390/ma11101993>
38. Misch CE, Qu Z, Bidez MW. Mechanical properties of trabecular bone in the human mandible: implications for dental implant treatment planning and surgical placement. *J Oral Maxillofac Surg.* 1999;57:700–6. [https://doi.org/10.1016/s0278-2391\(99\)90437-8](https://doi.org/10.1016/s0278-2391(99)90437-8)
39. Noguchi H, Koda M, Funayama T, Kumagai H, Saito J, Mannoji C, et al. Regenos spacers are not suitable for open-door laminoplasty because of serious adverse events caused by their insufficient mechanical strength. *J Clin Neurosci.* 2018;56:50–5. <https://doi.org/10.1016/j.jocn.2018.07.015>
40. Funayama T, Noguchi H, Kumagai H, Sato K, Yoshioka T, Yamazaki M. Unidirectional porous beta-tricalcium phosphate and hydroxyapatite artificial bone: a review of experimental evaluations and clinical applications. *J Artif Organs.* 2021;24:103–10. <https://doi.org/10.1007/s10047-021-01270-8>
41. Noguchi H, Koda M, Funayama T, Kumagai H, Abe T, Nagashima K, et al. Bone bonding, displacement, and absorption in cases of double-door laminoplasty with unidirectional porous hydroxyapatite spacers. *J Clin Neurosci.* 2019;62:46–52. <https://doi.org/10.1016/j.jocn.2019.01.012>
42. Ikumi A, Iwasashi M, Muramatsu T, Li S, Hangai M, Sakane M. Clinical and radiological evaluation of unidirectional porous hydroxyapatite (Regenos®) for intra-articular calcaneal fracture with large bone defect. *Foot Ankle.* 2014;J7:5.
43. Iwasashi M, Muramatsu T, Sakane M. Radiological and histological evaluation of Regenos® which implanted in human radial fracture: a clinical case report. *Key Eng Mater.* 2012;529–530:313–6.